

4-3-2023

Gravity Waves Emitted from Kelvin-Helmholtz Instabilities

Alan Z. Liu

Embry-Riddle Aeronautical University, liuz2@erau.edu

Wenjun Dong

Embry-Riddle Aeronautical University, Global Atmospheric Technologies and Sciences, National Center for Atmospheric Research

David C. Fritts

Embry-Riddle Aeronautical University, Global Atmospheric Technologies and Sciences

Thomas S. Lunda

Global Atmospheric Technologies and Sciences

Han-Li Liu

National Center for Atmospheric Research

Follow this and additional works at: <https://commons.erau.edu/publication>



Part of the [Atmospheric Sciences Commons](#)

Scholarly Commons Citation

Dong, W., Fritts, D. C., Liu, A. Z., Lund, T. S., & Liu, H.-L. (2023). Gravity waves emitted from Kelvin-Helmholtz instabilities. *Geophysical Research Letters*, 50, e2022GL102674. <https://doi.org/10.1029/2022GL102674>

This Article is brought to you for free and open access by Scholarly Commons. It has been accepted for inclusion in Publications by an authorized administrator of Scholarly Commons. For more information, please contact commons@erau.edu.

Geophysical Research Letters[®]



RESEARCH LETTER

10.1029/2022GL102674

Gravity Waves Emitted From Kelvin-Helmholtz Instabilities

Wenjun Dong^{1,2,3} , David C. Fritts^{1,2} , Alan Z. Liu¹ , Thomas S. Lund², and Han-Li Liu³ 

Key Points:

- Kelvin-Helmholtz instabilities (KHI) generated by a stratified shear layer induce gravity waves (GWs) that penetrate to high altitudes
- KHI-radiated GWs may be a major influence of near-stationary shears at high altitudes to which they cannot readily propagate directly
- GWs generated by KHI can account for “fishbone” structures seen in vertical profiling

Correspondence to:

A. Z. Liu,
Liuz2@erau.edu

Citation:

Dong, W., Fritts, D. C., Liu, A. Z., Lund, T. S., & Liu, H.-L. (2023). Gravity waves emitted from Kelvin-Helmholtz instabilities. *Geophysical Research Letters*, 50, e2022GL102674. <https://doi.org/10.1029/2022GL102674>

Received 26 DEC 2022

Accepted 3 APR 2023

Author Contributions:

Conceptualization: Wenjun Dong, David C. Fritts, Alan Z. Liu

Data curation: Wenjun Dong, Thomas S. Lund

Formal analysis: Wenjun Dong, David C. Fritts, Alan Z. Liu

Funding acquisition: David C. Fritts, Alan Z. Liu

Investigation: Wenjun Dong, David C. Fritts, Alan Z. Liu, Thomas S. Lund, Han-Li Liu

Methodology: Wenjun Dong, David C. Fritts, Thomas S. Lund, Han-Li Liu

Resources: Wenjun Dong

Software: Wenjun Dong, Thomas S. Lund

Supervision: Wenjun Dong, David C. Fritts, Alan Z. Liu

Validation: Wenjun Dong, David C. Fritts, Han-Li Liu

Visualization: Wenjun Dong

© 2023. The Authors.

This is an open access article under the terms of the [Creative Commons Attribution-NonCommercial-NoDerivs License](https://creativecommons.org/licenses/by/4.0/), which permits use and distribution in any medium, provided the original work is properly cited, the use is non-commercial and no modifications or adaptations are made.

¹Department of Physical Sciences, Center for Space and Atmospheric Research (CSAR), Embry-Riddle Aeronautical University, Daytona Beach, FL, USA, ²Global Atmospheric Technologies and Sciences (GATS), Boulder, CO, USA, ³High Altitude Observatory, National Center for Atmospheric Research, Boulder, CO, USA

Abstract Fritts, Wang, Lund, and Thorpe (2022, <https://doi.org/10.1017/jfm.2021.1085>) and Fritts, Wang, Thorpe, and Lund (2022, <https://doi.org/10.1017/jfm.2021.1086>) described a 3-dimensional direct numerical simulation of interacting Kelvin-Helmholtz instability (KHI) billows and resulting tube and knot (T&K) dynamics that arise at a stratified shear layer defined by an idealized, large-amplitude inertia-gravity wave. Using similar initial conditions, we performed a high-resolution compressible simulation to explore the emission of GWs by these dynamics. The simulation confirms that such shear can induce strong KHI with large horizontal scales and billow depths that readily emit GWs having high frequencies, small horizontal wavelengths, and large vertical group velocities. The density-weighted amplitudes of GWs reveal “fishbone” structures in vertical cross sections above and below the KHI source. Our results reveal that KHI, and their associated T&K dynamics, may be an important additional source of high-frequency, small-scale GWs at higher altitudes.

Plain Language Summary A high-resolution compressible atmosphere model is applied to explore gravity wave emissions from a shear with Kelvin-Helmholtz Instability initiated by a three-dimensional, small-amplitude initial noise field in velocity, such as must always occur in the atmosphere. Simulations reveal that a wind shear with an amplitude of 65 m/s and a half-width of 0.8 km can induce strong Kelvin-Helmholtz Instability dynamics, which can further emit gravity waves having periods of ~10–20 min and horizontal wavelengths of ~20 km. These gravity waves have high frequencies and small horizontal scales. The density-weighted amplitudes of gravity waves created a “fishbone” structure in z-t plots due to upward- and downward-propagating gravity waves arising at the layer of Kelvin-Helmholtz Instability. Our results demonstrate that Kelvin-Helmholtz Instability and the resulting instability dynamics may be a prevalent source of gravity waves impacting higher altitudes.

1. Introduction

It has been recognized for many years that gravity waves (GWs) play fundamental roles in a wide range of atmospheric processes from the surface to very high altitudes (Fritts & Alexander, 2003). Understanding these processes and their influences requires more complete quantification of the mechanisms by which GWs are generated, together with their characteristics, distributions, and responses in a wide range of environments. Of the recognized GW sources, secondary GWs (GWs) are important because they extend the vertical range of GW influences into the thermosphere and can do so quickly because of their often-large scales and vertical group velocities. Importantly, however, their generation mechanisms are the least rigorously studied and understood to date. This is because their sources are challenging to quantify observationally, and their associated dynamics are intrinsically nonlinear.

Our focus in this paper is on GWs excited by Kelvin-Helmholtz instabilities (KHI), which have been less studied to date. Theory and modeling have suggested that GWs are excited by two types of instabilities. First, GW “self-acceleration” (SA) instability dynamics due to localized and transient GW/mean-flow interactions excite GWs having spatial scales dictated by the geometry and timescale of the local induced body forcing (Dong et al., 2020, 2021, 2022; Fritts et al., 2020). Importantly, this mechanism can lead to GW generation prior to, and perhaps in the absence of, primary GW instabilities. Second, where KHI arise in an unstable shear due in part to inertia gravity waves (IGWs), they can radiate smaller-scale and higher-frequency GWs. As examples, previous studies have suggested that GWs can be emitted from small-scale KHI, localized KHI “packets,” and turbulent wakes (e.g., Abdilghanie & Diamessis, 2013; Bühler et al., 1999; Chimonas & Grant, 1984a, 1984b;

Writing – original draft: Wenjun Dong, David C. Fritts
Writing – review & editing: David C. Fritts, Alan Z. Liu, Thomas S. Lund, Han-Li Liu

Fritts, 1982, 1984). Relative to the more widely recognized GW sources, such KHI sources have been recognized for many years, but remain one of the least quantified GW sources.

KHI has been observed in polar mesospheric clouds and in airglow layers in the mesosphere (Fritts et al., 2019; Hecht et al., 2021; Kjellstrand et al., 2022). They often arise where vertical gradients of horizontal winds are enhanced due to high-frequency GWs with periods of several minutes and IGWs attaining enhanced local shears at large amplitudes. IGWs having frequencies near the inertial frequency can lead to self-induced KHI (Lelong & Dunkerton, 1998; Thorpe, 1999). The subharmonic interaction of KH modes (Davis & Peltier, 1979) and “envelope” radiation (Fritts, , 1984; Scinocca & Ford, 2000) are believed to be essentially GW excitation by the packet-scale motions accompanying coherent KH billows evolving in an unstable shear layer. Importantly, however, these early studies were limited to quasi-linear theory or modeling with very limited resolution.

Despite the considerable evidence for these expected GW sources, no simulations resolving these dynamics have been reported to date, perhaps due to the large domains and computational resources required to explore their responses at the high Re and moderate Ri required. To our knowledge, this paper is the first to describe GWs emitted by an approximate, large-amplitude unstable shear layer using a high-resolution nonlinear atmospheric model. A brief description of Complex Geometry Compressible Atmosphere Model (CGCAM) and its initial conditions is provided in Section 2. Section 3 describes results for the KHI-radiated GWs. Our discussion is provided in Section 4, and Section 5 presents our summary and conclusions.

2. Modal Configuration

2.1. Compressible Equations

The CGCAM solves the 3-D nonlinear and compressible Navier-Stokes equations written in strong conservation law (flux) form as follows:

$$\frac{\partial \rho}{\partial t} + \frac{\partial(\rho u_j)}{\partial x_j} = 0 \quad (1)$$

$$\frac{\partial(\rho u_i)}{\partial t} + \frac{\partial(\rho u_i u_j)}{\partial x_j} = -\frac{\partial p}{\partial x_i} - \rho g \delta_{i3} + \frac{\partial \sigma_{ij}}{\partial x_j} \quad (2)$$

$$\frac{\partial(\rho E)}{\partial t} + \frac{\partial[(\rho E + p)u_j]}{\partial x_j} = -\rho g u_3 + \frac{\partial(u_i \sigma_{ij})}{\partial x_j} - \frac{\partial q_j}{\partial x_j} \quad (3)$$

where σ_{ij} and q_j are the viscous stress and thermal conduction, respectively, defined as

$$\sigma_{ij} = \mu \left[\left(\frac{\partial u_i}{\partial x_j} + \frac{\partial u_j}{\partial x_i} \right) - \frac{2}{3} \left(\frac{\partial u_k}{\partial x_k} \right) \delta_{ij} \right] \quad (4)$$

$$q_j = -\kappa \frac{\partial T}{\partial x_j} \quad (5)$$

and where μ is the dynamic viscosity, κ is the thermal conductivity, δ_{ij} is the Kronecker delta, ρ is density, and g is the gravitational acceleration. μ and κ depend on the temperature through Sutherland's Law (White, 1974). For the high frequency motions considered here, the Coriolis force can be ignored.

The solution variables are ρ , the momentum per unit volume, ρu_i or $(\rho u, \rho v, \rho w)$, and the total energy $E = e + u_k u_k / 2 = c_v T + u_k u_k / 2$, with velocity components (u_i, u_j, u_k) along (x, y, z) , e is the potential energy. Also $c_v = R/\gamma - 1$ is the specific heat at constant volume and T is the temperature. The compressible equation set is discretized using a second-order finite-volume scheme identical to the method discussed by Felten and Lund (2006). Time advancement is achieved via a third-order accurate Runge-Kutta scheme. Additional details for CGCAM are provided by Dong et al. (2020) and Lund et al. (2020).

2.2. Initial and Boundary Conditions

We specify initial background conditions approximating a large-amplitude shear with a vertical wavelength of ~ 15 km accounting for the horizontal velocity and temperature profiles. The initial conditions are similar to those

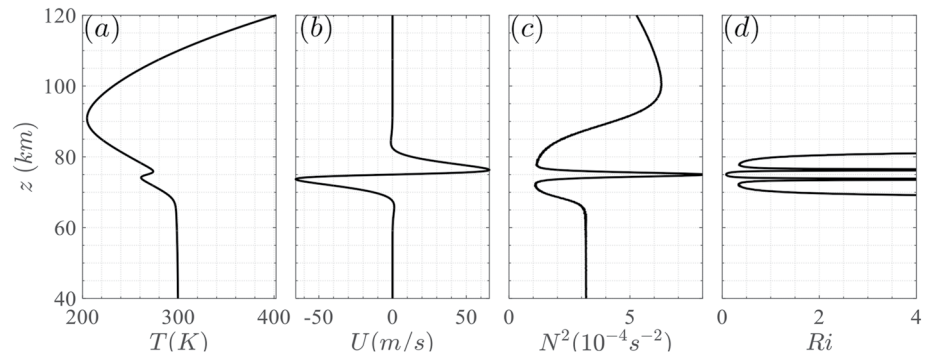


Figure 1. Initial fields in $T(z)$ and $U(z)$, and the resulting $N^2(z)$ and $Ri(z)$.

in Fritts, Wang, Lund, and Thorpe (2022) and Fritts, Wang, Thorpe, and Lund (2022), who employed a direct numerical simulation to explore the dynamics and energetics of KHI “tube and knot” (T&K) dynamics that arise where KH billows are mis-aligned along their axes. We use the same initial condition forms to allow similar responses as the source of GWs in this study, specified as

$$U(z) = U_0 \cos \left[\frac{\pi(z - z_0)}{15 \text{ km}} \right] \tan h \left(\frac{z - z_0}{h} \right) \quad (6)$$

$$N^2(z) = N_0^2 + (N_m^2 - N_0^2) \sec h^2 \left(\frac{z - z_0}{h} \right) \quad (7)$$

In this application, $z_0 = 75 \text{ km}$ is the center of shear source, $h = 800 \text{ m}$ is the half depth of the shear layer implying an expected KHI horizontal scale $\lambda_h \sim 4\pi h \sim 10 \text{ km}$, and the shear amplitude is $U_0 = \sim 65 \text{ m/s}$. We also assume $Re = U_0 h / \nu = 2,000$ in order to constrain the required resolution and resolve the KHI and turbulence dynamics described via the CGCAM large-eddy simulation scheme. This results in a turbulent kinematic viscosity of $\nu = U_0 h / 2,000 \sim 10 \text{ m}^2/\text{s}$. We also assume $N_0^2 = 0.0001 \text{ s}^{-2}$ and $N_m^2 = 0.0008 \text{ s}^{-2}$, given that KHI inevitably arise where GWs yield enhanced shears at peaks in the local stratification. The initial profiles are shown in Figure 1 and incorporated into the mean state. The background has a shear of 130 m/s over 5 km , which results in a Richardson number of 0.15 . This value is in the domain of KHI ($0 < Ri < 0.25$) and supports our claim that the selected wave case falls within the known criteria for KHI production.

The simulation was performed in a computational domain having dimensions $100 \times 100 \times 140 \text{ km}$ (x , y , and z) with isotropic resolution of 50 m at the shear source altitude, and exponential mesh stretching near the upper and lower boundaries to reduce computational demands. Periodic boundary conditions are used at the lateral boundaries. An isothermal no-stress wall condition is used at the lower boundary, and a characteristic radiation condition is used at the upper boundary. The vertical boundary conditions are supplemented with sponge layers of 20-km depths to absorb outgoing GWs and Acoustic Waves.

3. Results

Perturbation u' , w' , and T'/T_0 (top to bottom) are shown with x - z cross sections of the 3-D simulation fields at $y = 0$ and at 18, 25, 38, 50, and 62 min after initiation in Figure 2. The KHI arise in the shear centered at the minimum Ri at $z = 75 \text{ km}$ (see Figure 1b). The strong initial shear yields deep KH billows at expected $\sim 10 \text{ km}$ horizontal scales. By 25 min, the KH billows exhibit initial instabilities, breaking via secondary convective instabilities, and initial GW radiation to higher and lower altitudes. By 38 min, the KH billows have largely broken down and radiating GWs are more prominent. These have primary alignments toward negative (positive) x above (below) the initial shear layer due to the positive (negative) U above (below) the source shear at earlier times. GWs having opposite propagation directions also emerge as the breaking KHI expand vertically. The initial KHI perturbations largely disappear by 50 min, and the dominant KHI-driven GW generation almost ceases by $\sim 62 \text{ min}$, but the GWs excited by the initial, smaller-scale KHI dynamics achieve large amplitudes that can have significant influences at higher altitudes thereafter. Importantly, these GWs have horizontal scales of $\sim 30\text{--}50 \text{ km}$ and vertical scales of $\sim 10\text{--}25 \text{ km}$ above $\sim 90 \text{ km}$, so also have relatively high intrinsic frequencies, due to the

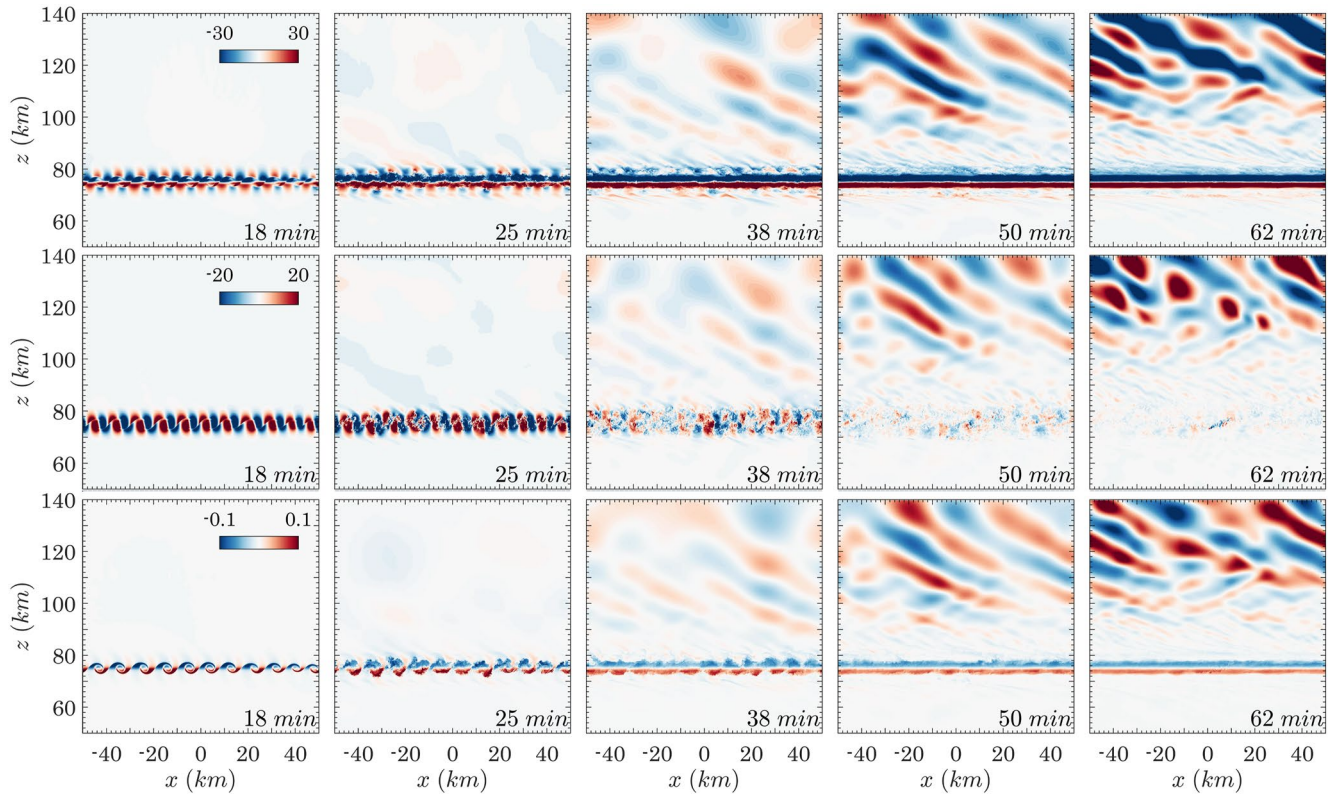


Figure 2. x - z cross sections of (top to bottom) u' (m/s), w' (m/s), and T'/\bar{T} at 18, 25, 38, 50, and 62 min (left to right).

transient KHI evolution and breakdown. This implies large corresponding energy and momentum fluxes that can induce potentially significant influences at higher altitudes and perhaps be competitive with GWs responses from other sources.

Spectra are useful to identify the onset of nonlinear transfers across a broad range of scales. Spectra of $u'w'$ computed over $70 \text{ km} \leq z \leq 80$ and $90 \text{ km} \leq z \leq 120$ km at $t = 25, 38, 50,$ and 62 min are displayed in the right panels of Figure 3. Considering first the spectra of $70 \text{ km} \leq z \leq 80$ km, at 25 min (blue lines), the onset of strong KHI and the dynamics accounting for their breakdown yield strong peaks at the KHI wavelength and its harmonics, and spectral slopes at larger k approaching $-5/3$ at resolved scales. This apparent inertial range also extends to larger amplitudes and somewhat smaller scales at later times. Spectral amplitudes fall sharply above wavenumbers of ~ 20 rad/km and exhibit much steeper slopes of -7 within the viscous range. These spectra suggest that the KHI and their instability dynamics accounting for GW radiation are sufficiently resolved for our purposes here.

Referring to the spectra from $90 \text{ km} \leq z \leq 120$ km, we see that $\langle u'w'(k) \rangle$ has a peak value at ~ 38 min and largely reflects the radiated GW wavenumber dependence in k with the major peak at the GW $\lambda_x = 2\pi/k = \sim 20$ km. At 38 min, initial GWs appear above 90 km, the GW amplitudes and their corresponding spectral densities increase with time, and these spectral features are consistent with GW emissions from KHI at lower altitudes. Compared to the spectral at altitudes of $70 \text{ km} \leq z \leq 80$ km, the $-5/3$ slope at altitudes of $90 \text{ km} \leq z \leq 120$ km begins at a larger k and has a narrower k range where it converges. The kinematic viscosity plays a key role in energy transfer, and it increases with decreasing density. Large kinematic viscosity at altitude increases the wavelength of the transition point between $-5/3$ and -7 slopes, that is, larger eddies are being dissipated through viscosity as the altitude and kinematic viscosity increases.

Figure 4 (top) shows scaled horizontal wind perturbations $\sqrt{\rho(z)/\rho(z=0)}u'$ in x - z cross sections at 18, 25, 38, 50, and 62 min. Note that the contour scales at altitudes of 70–80 km are reduced by factors of 40 in order to clearly reveal the GWs emitted from the KHI. Figure 4 also shows z - t plots of $\sqrt{\rho(z)/\rho(z=0)}u'$, $\sqrt{\rho(z)/\rho(z=0)}w'$, and $\sqrt{\rho(z)/\rho(z=0)}T'/\bar{T}$. The density-weighted GW amplitudes exhibit a “fishbone” structure in z - t plots due to

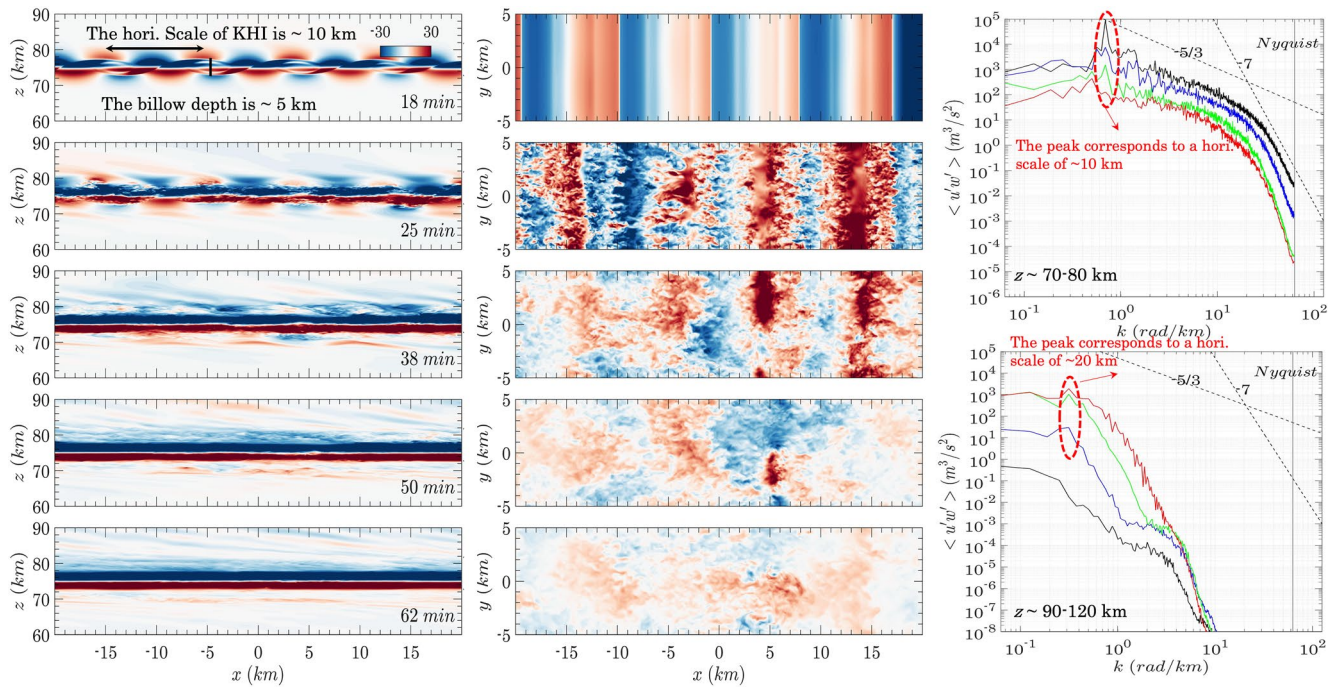


Figure 3. x - z (left) and x - y (middle) subdomain cross sections of u' (m/s) at 18, 25, 38, 50, and 62 min (top to bottom). (right) Spectra of $u'w'$ computed over $|x| \leq 50$ km, and $70 \text{ km} \leq z \leq 80$ km (top) and $90 \text{ km} \leq z \leq 120$ km (bottom). Times of 25, 38, 50, and 62 min are shown in black, blue, green, and red. Slopes of $-5/3$ and -7 are shown as dashed black lines at upper right in each panel. The Nyquist frequency is shown as gray solid line in each spectral plot.

upward- and downward-propagating GWs arising from the KHI source. Specifically, GWs with downward phase progression are seen above the KHI source, and GWs with upward phase progression are seen below the KHI source.

The GW parameters are quantified via a 2-D Fourier transform of $\sqrt{\rho(z)/\rho(z=0)}u'$ below and above the KHI source region and are shown in the first row in Figure 5. The downward propagating GWs have a strong peak at $\tau = 10$ min and $|\lambda_z| = 20$ km and a weaker peak at $\tau = 20$ min and $|\lambda_z| = 20$ km. The upward propagating GWs also have two peaks, with the strong peak at $\tau = 20$ min and $|\lambda_z| = 20$ km. The differences between upward- and downward-propagating GWs might be due to the variations in N , thus the various filtering effects for various GW components.

To verify this, a case is initiated in an isothermal background. Apart from the background temperature profile, other configurations are the same as in Case 1 (the first case we performed). The 2-D Fourier transform for $\sqrt{\rho(z)/\rho(z=0)}u'$ at z - t slice at $20 \text{ km} < z < 60$ and $90 \text{ km} < z < 130$ km is shown in the bottom panel of Figure 5. As we expected, the upward-propagating and downward-propagating GWs have almost same characteristics. The horizontal and vertical scales (~ 10 km) of GWs have the same value as the KHI scale (~ 10 km). The vertical scale of GWs has been shown in the bottom panel in Figure 5, the horizontal scale of GWs can be derived according to GW dispersion relationship (Equation 23 from Fritts and Alexander (2003)). This case shows the generated upward- and downward-propagating GWs exhibit near-perfect symmetry around the KHI axis, and those GWs have horizontal and vertical scales comparable to that of KHI.

4. Discussion

Our results demonstrate that KHI and resulting turbulence dynamics can play a key role in GWs arising in a shear environment. It is suggested that KHI may naturally constitute an important widespread source of high-frequency small-scale GWs. Specifically, intense, large-scale KHI dynamics at lower altitudes likely act as sources of small-scale GWs reaching the mesosphere, thermosphere, and ionosphere (MTI), and as potential seeds of plasma instabilities at higher altitudes, as demonstrated by Hysell et al. (2018). Our findings indicate that shear-induced KHI may be a potential contributing factor to the high-frequency gravity waves (GWs) with

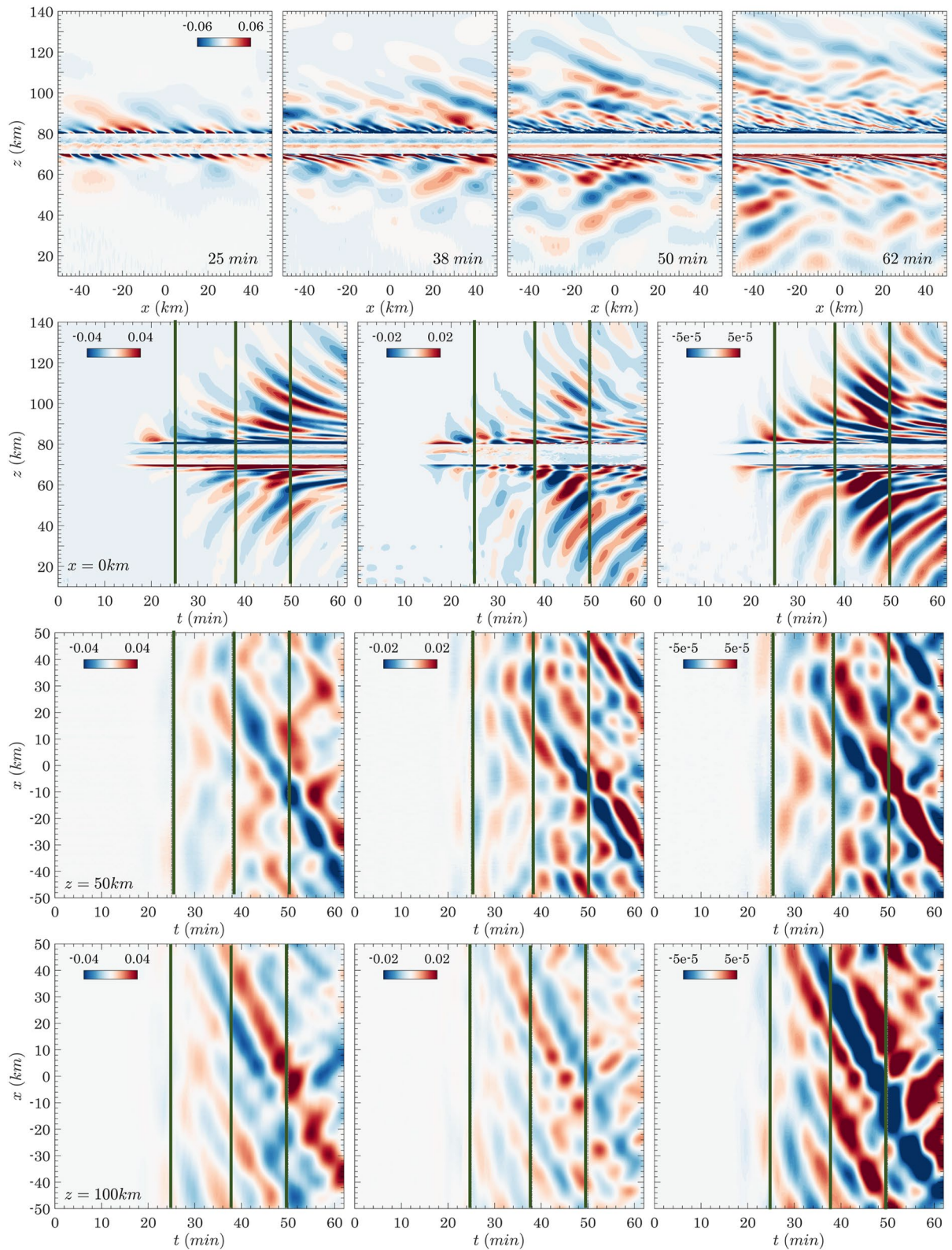


Figure 4. (top row) x - z cross sections of $\sqrt{\rho(z)/\rho(z=0)}u'$ at 25, 38, 50, and 62 min (left to right), (second row) vertical-temporal slices of $\sqrt{\rho(z)/\rho(z=0)}u'$, $\sqrt{\rho(z)/\rho(z=0)}w'$, and $\sqrt{\rho(z)/\rho(z=0)}T'/T$ (left to right) at $x = 0$ km, and (third and fourth rows) zonal-temporal slice at $z = 50$ and 100 km (left and right). The green lines denote 25, 38, and 50 min. Note that the contour scales at altitudes of 70–80 km in the top two rows are reduced by factors of 40 in order to clearly reveal the GWs emitted from the Kelvin-Helmholtz instabilities.

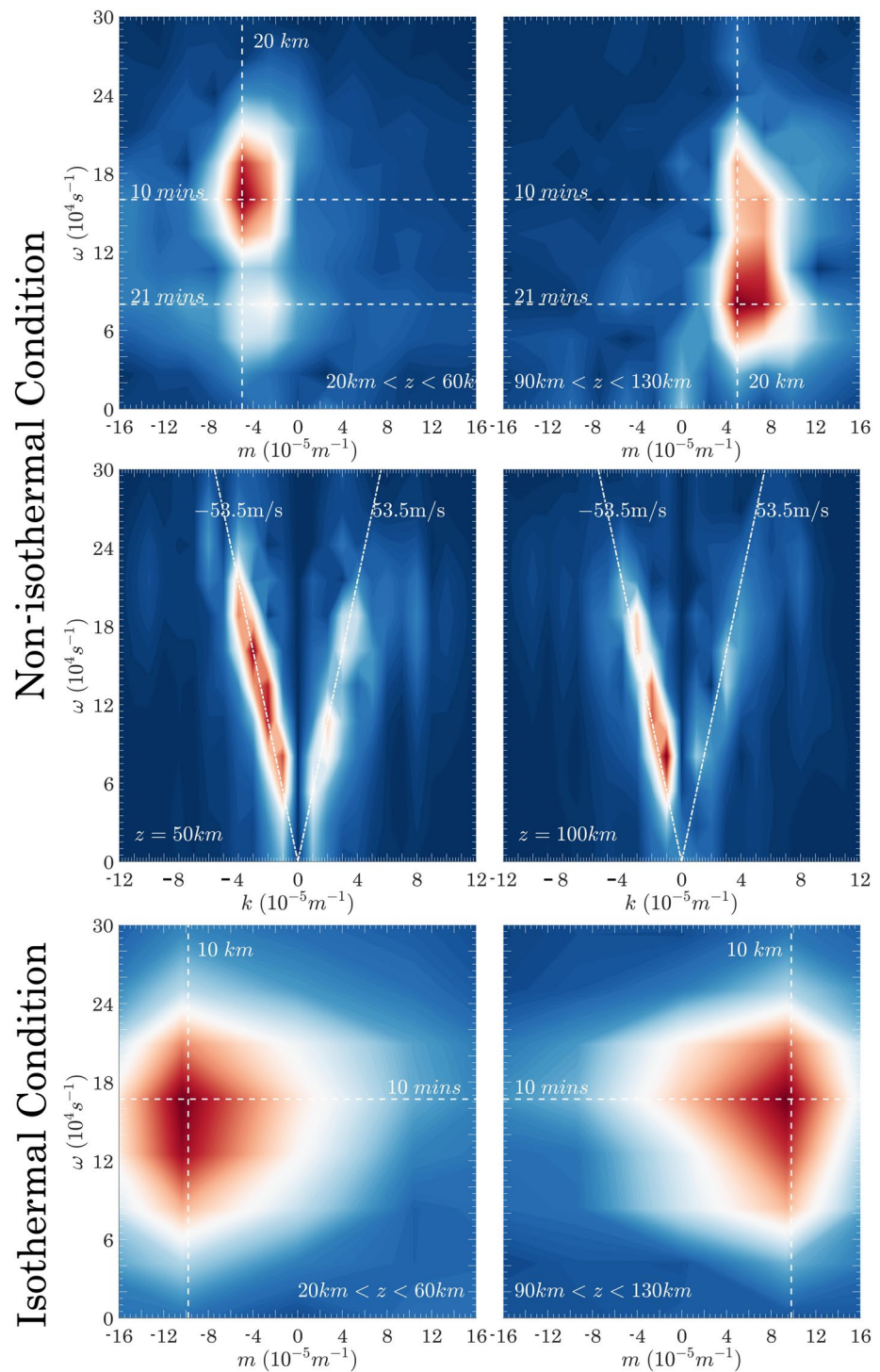


Figure 5. The first row is the 2-D Fourier transform of $\sqrt{\rho(z)/\rho(z=0)}u'$ at a z - t slice at $20 \text{ km} < z < 60$ and $90 \text{ km} < z < 130 \text{ km}$ (left and right). The second row is the 2-D Fourier transform of $\sqrt{\rho(z)/\rho(z=0)}u'$ at x - t slice at $z = 50$ and 100 km (left and right). The third row is same as row 1, but for a case with isothermal background ($T(z) = 300 \text{ K}$). The power spectral densities have been normalized to vary from 0 to 1. White dashed lines in the second row indicate lines of constant horizontal phase speed.

short wavelengths ranging between 15 and 25 km that have been observed in the mesosphere (Ejiri et al., 2003; Medeiros et al., 2007; Narayanan & Gurubaran, 2013). Given these new insights, multi-scale modeling efforts are needed to explore their potential to drive small-scale GWs and plasma turbulence extending to high altitudes in the MTI for a diverse range of environments.

This paper provides only preliminary results of GWs generated in the shear environments. Questions remain as to what mechanism is responsible for the GWs characteristics. The underlying physics becomes more complicated because the GW emissions are linked to different coherent vortical structures of the multi-scale KHI and successive turbulence dynamics. The mechanism likely depends on complex multi-scale dynamics, and will surely exhibit strong dependence of shear and KHI properties, including Re , viscosity, the degree of spatial localization of the shear, and their spectral domain. Despite the valuable insights provided by this study on KHI-radiated GWs, a number of critical aspects of these underlying physics have not yet been addressed. Further analyses will be needed to determine the roles of the various governing parameters in determining the GW characteristics, likely including the following:

1. The dependence on shear parameters, such as the forms of shear, environments, and localization that accompany weaker and smaller-scale superposed GWs, will define the characteristics, scales, and propagation of the GWs. Measurements of shears have been described in previous studies, such as Larsen (2002) and England et al. (2022), with shears in laminar flow possibly resulting from GWs propagating through a tidal background, where shears combine for a given phase of the respective waves.
2. Dependence on the Re and Ri that characterize the initial wind shears, as these will surely influence the scales and character of the GW responses but have not been explored to date.
3. The dependence of GW generation on the characteristics and scales of KHI interactions leading to tube and knot (T&K) dynamics. Recent studies by Fritts, Wang, Lund, and Thorpe (2022) and Fritts, Wang, Thorpe, and Lund (2022) have shown that T&K comprise strong and complex vortex interactions that accompany misaligned KH billows and accelerate the transition to turbulence compared to secondary instabilities of individual KH billows. These T&K dynamics are important processes in KHI evolution, and their impact on the excitation of GWs is not yet fully understood.

5. Summary and Conclusions

We described an initial high-resolution simulation of GW radiation accompanying KHI in an idealized shear environment. Our results indicate that the strong KHI and turbulence dynamics induced by shear can lead to significant generation of small-scale, high-frequency GWs. Our specific findings include the following:

1. The strong KHI and turbulence dynamics induced by shear can emit GWs having periods of ~ 10 – 20 min and horizontal wavelengths of ~ 10 – 20 km.
2. The density-weighted GW amplitudes created a “fishbone” structure in z - t plots arising where upward- and downward-propagating GWs arise at a central source, that is, the shear layer.
3. KHI may naturally constitute an important source of high-frequency, smaller-scale GWs potentially propagating to much higher altitudes.

As discussed above, there are many aspects of these dynamics that are beyond the scope of this paper that need to be explored further in order to assess their importance in coupling into the mesosphere and lower thermosphere.

Data Availability Statement

The data needed to reproduce each figure is available at <https://doi.org/10.6084/m9.figshare.20387187.v1>. If you require complete simulation data for your study, please reach out to Wenjun Dong at dongw1@erau.edu for assistance. Simulation data is provided in a *vtk* file format and can be opened by the open source software ParaView version 5.10 (Ahrens et al., 2005; Ayachit, 2015), which is available under the BSD license at <https://www.paraview.org/download/>. The ParaView Guide can be downloaded from <http://www.paraview.org/download/>.

Acknowledgments

We are immensely grateful to the anonymous reviewer and Prof. Gary Swenson for taking the time to review our paper and provide valuable comments and suggestions. Their feedback has been crucial in improving the quality of our work. Research described here was supported by the Air Force Office of Scientific Research Grant FA9550-18-1-0009 and NSF Grants AGS-1759471, AGS-2032678, AGS-2131350 and AGS-2128443 cited in GEMS. We also acknowledge the Embry-Riddle Aeronautical University for access to a supercomputer platform that allowed the CGCAM simulations reported here. The National Center for Atmospheric Research is a major facility sponsored by the National Science Foundation under Cooperative Agreement No. 1852977.

References

- Abdilghanie, A. M., & Diamessis, P. J. (2013). The internal gravity wave field emitted by a stably stratified turbulent wake. *Journal of Fluid Mechanics*, *720*, 104–139. <https://doi.org/10.1017/jfm.2012.640>
- Ahrens, J., Geveci, B., & Law, C. (2005). *ParaView: An end-user tool for large data visualization, visualization handbook*. Elsevier. <https://doi.org/10.1016/B978-012387582-2/50038-1>
- Ayachit, U. (2015). *The ParaView guide: A parallel visualization application*. Kitware.
- Bühler, O., McIntyre, M. E., & Scinocca, J. F. (1999). On shear-generated gravity waves that reach the mesosphere. Part I: Wave generation. *Journal of the Atmospheric Sciences*, *56*(21), 3749–3763. [https://doi.org/10.1175/1520-0469\(1999\)056<3749:OSGGWT>2.0.CO;2](https://doi.org/10.1175/1520-0469(1999)056<3749:OSGGWT>2.0.CO;2)
- Chimonas, G., & Grant, J. R. (1984a). Shear excitation of gravity waves. Part 1: Modes of a two-scale atmosphere. *Journal of the Atmospheric Sciences*, *41*(15), 2269–2277. [https://doi.org/10.1175/1520-0469\(1984\)041<2269:SEOGWP>2.0.CO;2](https://doi.org/10.1175/1520-0469(1984)041<2269:SEOGWP>2.0.CO;2)
- Chimonas, G., & Grant, J. R. (1984b). Shear excitation of gravity waves. Part 2: Upscale scattering from Kelvin-Helmholtz waves. *Journal of the Atmospheric Sciences*, *41*(15), 2278–2288. [https://doi.org/10.1175/1520-0469\(1984\)041<2278:SEOGWP>2.0.CO;2](https://doi.org/10.1175/1520-0469(1984)041<2278:SEOGWP>2.0.CO;2)
- Davis, P., & Peltier, W. (1979). Some characteristics of the Kelvin-Helmholtz and resonant overreflection modes of shear flow instability and of their interaction through vortex pairing. *Journal of the Atmospheric Sciences*, *36*(12), 2394–2412. [https://doi.org/10.1175/1520-0469\(1979\)036<3C2394:SCOTKH%3E2.0.CO;2](https://doi.org/10.1175/1520-0469(1979)036<3C2394:SCOTKH%3E2.0.CO;2)
- Dong, W., Fritts, D. C., Hickey, M. P., Liu, A. Z., Lund, T. S., Zhang, S., et al. (2022). Modeling studies of gravity wave dynamics in highly structured environments: Reflection, trapping, instability, momentum transport, secondary gravity waves, and induced flow responses. *Journal of Geophysical Research: Atmospheres*, *127*(13), e2021JD035894. <https://doi.org/10.1029/2021JD035894>
- Dong, W., Fritts, D. C., Lund, T. S., Wieland, S. A., & Zhang, S. (2020). Self-acceleration and instability of gravity wave packets: 2. Two-dimensional packet propagation, instability dynamics, and transient flow responses. *Journal of Geophysical Research: Atmospheres*, *125*(3), e2019JD030691. <https://doi.org/10.1029/2019JD030691>
- Dong, W., Fritts, D. C., Thomas, G. E., & Lund, T. S. (2021). Modeling responses of polar mesospheric clouds to gravity wave and instability dynamics and induced large-scale motions. *Journal of Geophysical Research: Atmospheres*, *126*(13), e2021JD034643. <https://doi.org/10.1029/2021JD034643>
- Ejiri, M. K., Shiokawa, K., Ogawa, T., Igarashi, K., Nakamura, T., & Tsuda, T. (2003). Statistical study of short-period gravity waves in OH and OI nightglow images at two separated sites. *Journal of Geophysical Research: Atmospheres*, *108*(D21), 4679. <https://doi.org/10.1029/2002JD002795>
- England, S. L., Englert, C. R., Harding, B. J., Triplett, C. C., Marr, K., Harlander, J. M., et al. (2022). Vertical shears of horizontal winds in the lower thermosphere observed by ICON. *Geophysical Research Letters*, *49*(11), e2022GL098337. <https://doi.org/10.1029/2022GL098337>
- Felten, F. N., & Lund, T. S. (2006). Kinetic energy conservation issues associated with the collocated mesh scheme for incompressible flow. *Journal of Computational Physics*, *215*(2), 465–484. <https://doi.org/10.1016/j.jcp.2005.11.009>
- Fritts, D., Wang, L., Lund, T., & Thorpe, S. (2022). Multi-scale dynamics of Kelvin-Helmholtz instabilities. Part 1. Secondary instabilities and the dynamics of tubes and knots. *Journal of Fluid Mechanics*, *941*, A30. <https://doi.org/10.1017/jfm.2021.1085>
- Fritts, D., Wang, L., Thorpe, S., & Lund, T. (2022). Multi-scale dynamics of Kelvin-Helmholtz instabilities. Part 2. Energy dissipation rates, evolutions and statistics. *Journal of Fluid Mechanics*, *941*, A31. <https://doi.org/10.1017/jfm.2021.1086>
- Fritts, D. C. (1982). Shear excitation of atmospheric gravity waves. *Journal of the Atmospheric Sciences*, *39*(9), 1936–1952. [https://doi.org/10.1175/1520-0469\(1982\)039<1936:SEOAGW>2.0.CO;2](https://doi.org/10.1175/1520-0469(1982)039<1936:SEOAGW>2.0.CO;2)
- Fritts, D. C. (1984). Shear excitation of atmospheric gravity waves. Part II: Nonlinear radiation from a free shear layer. *Journal of the Atmospheric Sciences*, *41*(4), 524–537. [https://doi.org/10.1175/1520-0469\(1984\)041<0524:SEOAGW>2.0.CO;2](https://doi.org/10.1175/1520-0469(1984)041<0524:SEOAGW>2.0.CO;2)
- Fritts, D. C., & Alexander, M. J. (2003). Gravity wave dynamics and effects in the middle atmosphere. *Reviews of Geophysics*, *41*(1), L09801. <https://doi.org/10.1029/2001RG000106>
- Fritts, D. C., Dong, W., Lund, T. S., Wieland, S., & Laughman, B. (2020). Self-acceleration and instability of gravity wave packets: 3. Three-dimensional packet propagation, secondary gravity waves, momentum transport, and transient mean forcing in tidal winds. *Journal of Geophysical Research: Atmospheres*, *125*(3), e2019JD030692. <https://doi.org/10.1029/2019JD030692>
- Fritts, D. C., Miller, A. D., Kjellstrand, C. B., Geach, C., Williams, B. P., Kaifler, B., et al. (2019). PMC Turbo: Studying gravity wave and instability dynamics in the summer mesosphere using polar mesospheric cloud imaging and profiling from a stratospheric balloon. *Journal of Geophysical Research: Atmospheres*, *124*(12), 6423–6443. <https://doi.org/10.1029/2019JD030298>
- Hecht, J. H., Fritts, D. C., Gelinias, L. J., Rudy, R. J., Walterscheid, R. L., & Liu, A. Z. (2021). Kelvin-Helmholtz billow interactions and instabilities in the mesosphere over the Andes Lidar Observatory: 1. Observations. *Journal of Geophysical Research: Atmospheres*, *126*, e2020JD033414. <https://doi.org/10.1029/2020JD033414>
- Hysell, D., Larsen, M., Fritts, D., Laughman, B., & Sulzer, M. (2018). Major upwelling and overturning in the mid-latitude F region ionosphere. *Nature Communications*, *9*(1), 3326. <https://doi.org/10.1038/s41467-018-05809-x>
- Kjellstrand, C. B., Fritts, D. C., Miller, A. D., Williams, B. P., Kaifler, N., Geach, C., et al. (2022). Multi-scale Kelvin-Helmholtz instability dynamics observed by PMC Turbo on 12 July 2018: 1. Secondary instabilities and billow interactions. *Journal of Geophysical Research: Atmospheres*, *127*(18), e2021JD036232. <https://doi.org/10.1029/2021JD036232>
- Larsen, M. F. (2002). Winds and shears in the mesosphere and lower thermosphere: Results from four decades of chemical release wind measurements. *Journal of Geophysical Research*, *107*(A8), S1A 28-1–S1A 28-14. <https://doi.org/10.1029/2001JA000218>
- Lelong, M., & Dunkerton, T. (1998). Inertia-gravity wave breaking in three dimensions. Part I: Convectively stable waves. *Journal of the Atmospheric Sciences*, *55*(15), 2473–2488. [https://doi.org/10.1175/1520-0469\(1998\)055<3C2473:IGWBIT%3E2.0.CO;2](https://doi.org/10.1175/1520-0469(1998)055<3C2473:IGWBIT%3E2.0.CO;2)
- Lund, T. S., Fritts, D. C., Wan, K., Laughman, B., & Liu, H. (2020). Numerical simulation of mountain waves over the southern Andes. Part 1: Mountain wave and secondary wave character, evolutions, and breaking. *Journal of the Atmospheric Sciences*, *77*(12), 4337–4356. <https://doi.org/10.1175/JAS-D-19-0356.1>
- Medeiros, A. F., Takahashi, H., Buriti, R. A., Fechine, J., Wrasse, C. M., & Gobbi, D. (2007). MLT gravity wave climatology in the South America equatorial region observed by airglow imager. *Annales Geophysicae*, *25*(2), 399–406. <https://doi.org/10.5194/angeo-25-399-2007>
- Narayanan, V. L., & Gurubaran, S. (2013). Statistical characteristics of high frequency gravity waves observed by OH airglow imaging from Tirunelveli (8.7°N). *Journal of Atmospheric and Solar-Terrestrial Physics*, *92*, 43–50. <https://doi.org/10.1016/j.jastp.2012.09.002>
- Scinocca, J., & Ford, F. (2000). The nonlinear forcing of large-scale internal gravity waves by stratified shear instability. *Journal of the Atmospheric Sciences*, *57*(5), 653–672. [https://doi.org/10.1175/1520-0469\(2000\)057<3C0653:TNFOLS%3E2.0.CO;2](https://doi.org/10.1175/1520-0469(2000)057<3C0653:TNFOLS%3E2.0.CO;2)
- Thorpe, S. (1999). On the breaking of internal waves in the ocean. *Journal of the Atmospheric Sciences*, *29*(9), 2433–2441. [https://doi.org/10.1175/1520-0485\(1999\)029<3C2433:OTBOIW%3E2.0.CO;2](https://doi.org/10.1175/1520-0485(1999)029<3C2433:OTBOIW%3E2.0.CO;2)
- White, F. M. (1974). *Viscous fluid flow*. McGraw-Hill.